Journal of Applied Physics

High-pressure melt curve of shock-compressed tin measured using pyrometry and reflectance techniques

Cite as: J. Appl. Phys. **126**, 225103 (2019); https://doi.org/10.1063/1.5132318
Submitted: 17 October 2019 . Accepted: 25 November 2019 . Published Online: 10 December 2019

B. M. La Lone, P. D. Asimow, O. V. Fat'yanov, R. S. Hixson, G. D. Stevens, W. D. Turley, and L. R. Veeser

Journal of Applied Physics ARTICLE scitation.org/journal/jap

High-pressure melt curve of shock-compressed tin measured using pyrometry and reflectance techniques

Cite as: J. Appl. Phys. **126**, 225103 (2019); doi: 10.1063/1.5132318
Submitted: 17 October 2019 · Accepted: 25 November 2019 ·
Published Online: 10 December 2019

B. M. La Lone,[1,a)] P. D. Asimow,[2] O. V. Fat'yanov,[2] R. S. Hixson,[3] G. D. Stevens,[1] W. D. Turley,[1] and L. R. Veeser[1,3]

AFFILIATIONS

[1]Special Technologies Laboratory, Nevada National Security Site, Santa Barbara, California 93111, USA
[2]Division of Geological and Planetary Sciences, California Institute of Technology, Pasadena, California 91125, USA
[3]New Mexico Operations, Nevada National Security Site, Los Alamos, New Mexico 87544, USA

[a)]**Electronic mail:** lalonebm@nv.doe.gov.

ABSTRACT

We have developed a new technique to measure the melt curve of a shocked metal sample and have used it to measure the high-pressure solid-liquid phase boundary of tin from 10 to 30 GPa and 1000 to 1800 K. Tin was shock compressed by plate impact using a single-stage powder gun, and we made accurate, time-resolved radiance, reflectance, and velocimetry measurements at the interface of the tin sample and a lithium fluoride window. From these measurements, we determined temperature and pressure at the interface vs time. We then converted these data to temperature vs pressure curves and plotted them on the tin phase diagram. The tin sample was initially shocked into the high-pressure solid γ phase, and a subsequent release wave originating from the back of the impactor lowered the pressure at the interface along a constant entropy path (release isentrope). When the release isentrope reaches the solid-liquid phase boundary, melt begins and the isentrope follows the phase boundary to low pressure. The onset of melt is identified by a significant change in the slope of the temperature-pressure release isentrope. Following the onset of melt, we obtain a continuous and highly accurate melt curve measurement. The technique allows a measurement along the melt curve with a single radiance and reflectance experiment. The measured temperature data are compared to the published equation of state calculations. Our data agree well with some but not all of the published melt curve calculations, demonstrating that this technique has sufficient accuracy to assess the validity of a given equation of state model.

I. INTRODUCTION

The high-pressure phase diagram of materials is important in many disciplines, including earth and planetary science, materials science, astrophysics, armor penetration, and other military and defense applications. Consequently, extensive research has focused on measuring the temperature-pressure phase boundaries of various substances using both diamond anvil cell (DAC) and shock compression techniques. Melt conditions of shocked metals at high pressure are notoriously difficult to measure. Often, there is a substantial disagreement—sometimes thousands of degrees—between theory, static measurements, and dynamic measurements on the location of these boundaries.[1] Consequently, new and improved metal melt curve measurement techniques and a better understanding of the present methods are immediately needed. We have begun using a new technique to measure the melt curve of tin, and the method is applicable to other metals.

Static measurements of the solid-liquid phase boundary (the melt curve) and solid-solid phase changes in tin were first made in the early 1960s, typically using an anvil to pressurize a sample exposed to resistive heating while a thermocouple measured the temperature.[2–5] Melt was observed with techniques such as x-ray diffraction or a change in resistance or temperature as a function of pressure. More recently, extensive measurements have been made using a DAC or other static compression mechanisms with x-ray diffraction or other means of detecting melt.[6–9] In 2000, Mabire

and Héreil[10] observed shock waves created by flyer plate impact onto tin. Measured release wave velocity profiles, which contain sound speed information, had discontinuities that were used to infer melting at various pressures. However, temperatures were not measured. Using their data, they developed a three-phase equation of state (EOS) and calculated the phase diagram up to 70 GPa and 3000 K. In a separate study,[11] they reported the pyrometric temperature of shock-compressed tin measured at the interface between a tin sample and lithium fluoride window. They measured a melt temperature of 2110 ± 200 K at a pressure of 39 GPa, which agrees well with their model. A similar work by Anderson *et al.*[12] resulted in a phase diagram up to 10 GPa with more emphasis on the solid-solid transformation from the room-temperature β phase to the high-pressure γ phase. Anderson's model was based on a three-phase EOS model developed by Hayes[13] for bismuth. A recent work in shock waves by Chauvin *et al.*[14] used a thin carbon layer of known emissivity between the tin and the window to achieve a known emissivity and allow an accurate pyrometric temperature measurement. However, the carbon causes complexities that make it difficult to identify the temperature at which the release crosses the melt curve. In addition to the modeling by Mabire and Héreil[10] and Anderson *et al.*,[12] molecular dynamics calculations were performed by Bernard and Maillet[15] and density functional theory calculations by Mukherjee *et al.*[16] Figure 1 shows the experimental points for the static measurements, the Héreil dynamic point, theoretically calculated curves for the solid-liquid phase boundary in tin from various references, and the most recent SESAME EOS calculation.[17] There is substantial scatter in the experimental data and disagreement among the theories.

Our technique uses pyrometry and reflectance to measure the temperatures of shock-compressed tin across a large segment of the melt curve at the interface between the tin sample and a transparent window. The window is necessary to maintain elevated pressures at the surface of the sample after the arrival of the shock wave. In two separate measurements, we used a two-channel pyrometer to determine the spectral radiance of the sample surface and an integrating sphere (IS) reflectance technique to measure the sample emissivity $\varepsilon(t)$. (For opaque materials including metals, the emissivity ε and reflectance R are related by $\varepsilon = 1 - R$ from Kirchhoff's law of thermal radiation.) We generally perform these measurements in separate experiments; however, in one experiment, we performed both measurements simultaneously. From the radiance and emissivity, we determine the temperature $T(t)$ of the tin-window interface. In all experiments, we measure the interface velocity to obtain the pressure $P(t)$. The temperature and pressure measurements are combined to determine temperature vs pressure $T(P)$ along the melt boundary.

We have previously described a similar pyrometer[18] and the IS[19,20] technique that were combined to determine the temperatures of tin shocked by high explosives. In our prior work, the high-explosive drive was not one-dimensional, which complicated the analysis, and the pressures did not drop low enough to observe melting. Here, we applied these diagnostics to better-characterized loading conditions using tin targets impacted by flyer plates accelerated with a single-stage powder gun. Plate impact has two advantages: it maintains one-dimensional uniaxial strain loading during the experiment, and it enables more control over the pressure history in the samples so that we can create the temperature and pressure conditions necessary for melting to occur.

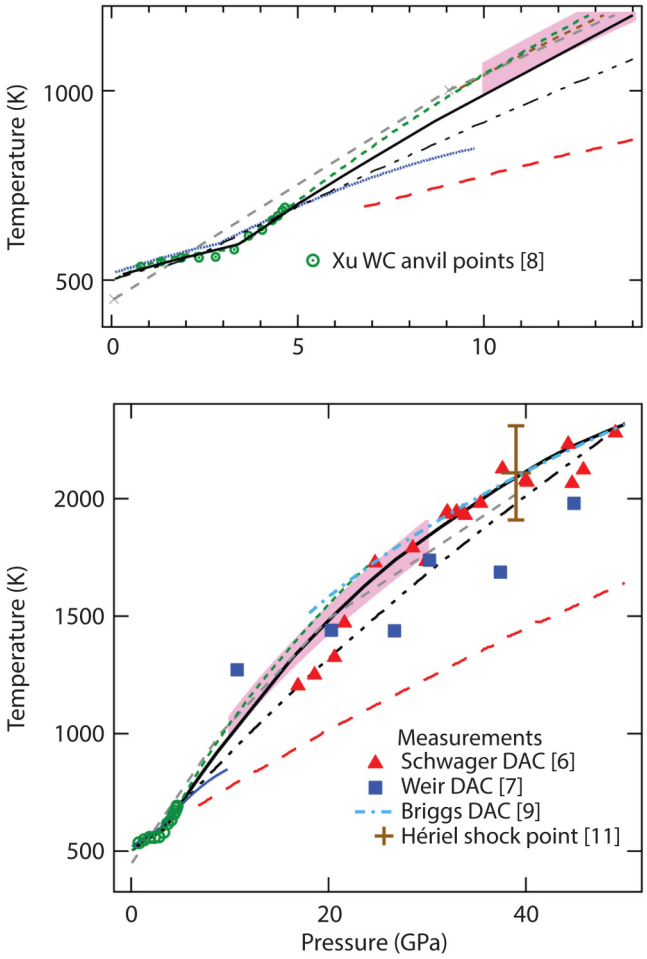

FIG. 1. The melt curve of tin. Points are published static temperature-vs-pressure measurements on the melt curve and the Mabire and Héreil[11] dynamic measurement. Curves from published modeling and theoretical calculations are from Mabire and Héreil[10] (solid black), Anderson *et al.*[12] (dotted blue at low pressures), Bernard *et al.*[15] (gray medium dashes), Mukherjee *et al.*[16] (red long dashes), and Xu *et al.*[8] (green small dashes at low pressures). The published Simon fit to the Briggs DAC measurements[9] (light blue dotted-dashed curve) and the SESAME 2169[17] data (dotted-dotted-dashed black) are also shown. The pink shaded line shows our data, and the curve thickness represents an upper limit of ±4% to the absolute uncertainty; see Sec. III. Substantial scatter in the experimental data and disagreement among the theories is evident.

II. EXPERIMENTAL DETAIL

Figure 2 shows a schematic of the experimental apparatus. A 1.3 mm thick, 32 mm diameter copper impactor, backed by syntactic foam (a low wave-impedance material), is launched to velocities ranging from 1.7 to 2.3 km/s using the 40 mm diameter, single-stage

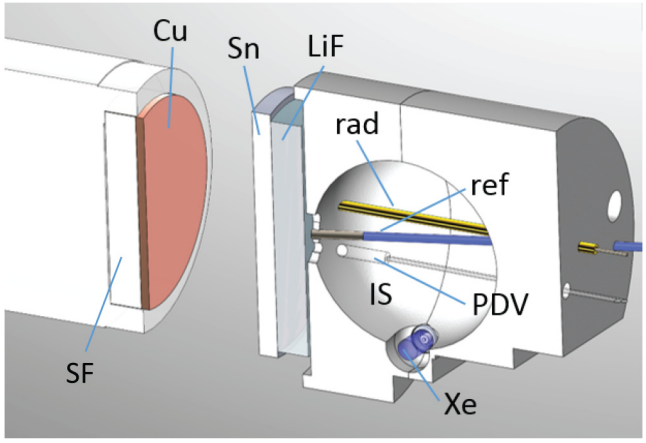

FIG. 2. Schematic diagram of the emissivity and radiance measurements. A copper plate (Cu) mounted to the face of a powder gun projectile and backed by syntactic foam (SF) impacts a tin (Sn) sample backed by a lithium fluoride (LiF) window and, for emissivity experiments, an integrating sphere (IS). The tin-LiF interface velocity is measured using a photonic Doppler velocimetry (PDV) probe. For pyrometry, thermal radiance from the tin is collected by a 400 μm diameter fiber (rad) and directed to an array of detectors. Each detector has a bandpass filter and a high-speed photodetector. For emissivity, a xenon flashlamp (Xe) illuminates the inside of the IS. Flashlamp light from the walls of the sphere is reflected from the tin-LiF interface, collected by the 1 mm diameter collection fiber (ref), and directed to the same or similar detectors. The emissivity is then determined from the reflectance. This figure depicts the one experiment during which reflectance (4E) and radiance (4R) were measured simultaneously by the radiance detectors; the radiance probe (rad) was placed off-center and away from the porthole in the IS, as shown in the figure. This radiance fiber was encapsulated in steel tubing to minimize the amount of unwanted xenon flashlamp light. In all other experiments, radiance (no IS, Xe, or ref) or emissivity (no rad) were measured separately.

powder gun at Caltech's Laboratory for Experimental Geophysics or by the 40 mm diameter single-stage powder gun operated by the Nevada National Security Site, Special Technologies Laboratory, in Goleta, California. The target is a 3 mm thick, 40 mm diameter tin sample[21] that is diamond turned on both sides to a specular finish and backed by either a 5 mm or 10 mm thick, 38 mm diameter [100] oriented lithium fluoride (LiF) window. The LiF window is attached to the tin with a thin (2–4 μm) Loctite 326 glue layer; both the glue and the window are transparent and nonemissive at shock pressures below 70 GPa.[22] The emissivity or radiance diagnostic, or in one case both, are mounted behind the window. The pyrometer has two channels, with wavelengths centered around 1300 (300) and 1600 (170) nm (bandpass widths in parentheses), respectively. Radiance in these short-wavelength infrared bands provides adequate signal-to-noise ratio from the amplified indium-gallium-arsenide (InGaAs) detectors at blackbody temperatures of 825 K or higher. We use a flashlamp–illuminated IS[20] technique (depicted in Fig. 2) to measure dynamic emissivity (reflectance) of the tin-LiF interface at detector wavelengths of 1300 (30) and 1550 (40) nm. Two wavelengths are sufficient for accurate temperature measurement (as opposed to the many bands often used in shock wave experiments) because the dynamic measurements of the sample emissivity at nearly the same wavelengths are included. The velocity history of the tin-LiF interface in each experiment is measured by photonic Doppler velocimetry (PDV).[23] In one experiment (4R and 4E), the thermal radiance was detected simultaneously with the emissivity measurement, as depicted in Fig. 2, by placing a 400 μm core fiber-optic radiance probe (in an extra penetration through the bottom of the IS) 8 mm from the center of the sphere bottom. This is far enough away from the porthole in the sphere that flashlamp light leaving the porthole to illuminate the tin cannot reflect from the surface and enter this fiber. Furthermore, this probe was encapsulated in steel tubing, and the outside of the IS was painted black where it was attached to the LiF for additional rejection of flashlamp light. The lamp light contamination in the radiance channels was less than 15% of the thermal radiance signal and was easily subtracted out because the lamp light levels change very little on the time scale of the experiment.

When the copper plate impacts the tin sample, a shock wave transits the tin layer and partially releases at the interface with the lower-impedance LiF window. We chose impact velocities such that the tin at the tin-LiF interface is initially compressed into the high-pressure solid γ (body-centered tetragonal) phase. A shock wave is also launched backward into the copper flyer upon impact. When the shock in the copper reaches the syntactic foam backing layer, it

TABLE I. Shock parameters for radiance and emissivity experiments. The interface pressure is determined immediately after the shock enters the LiF window. Pressures and temperatures upon initial melt are determined for each pair of reflectance and radiance measurements.

Experiment number	Cu projectile velocity (km/s)	Shock pressure in tin (GPa)	Interface velocity (km/s)	Initial pressure at interface (GPa)	Pressure at initial melt (GPa)	Temperature at initial melt (K)
1R	1.727	31.0	1.258	22.5	NA	NA
2R	1.965	36.7	1.424	26.3	13.1	1173
3R	2.108	40.3	1.516	28.7	18.9	1424
4R[a]	2.290	45.0	1.649	32.1	29.6	1821
1E	1.829	33.4	1.319	24.2		
2E	1.961	36.6	1.413	26.3		
3E	1.973	36.8	1.427	26.5		
4E[a]	2.290	45.0	1.649	32.1		

[a]4R and 4E were performed on the same experiment

sends a ramped release wave back through the copper and into the tin. This release wave reaches the tin-LiF interface about 300 ns after the initial shock wave. The initial shock wave increases the entropy of the tin, but it releases along an approximately constant entropy path (release isentrope) and, if the initial shock temperature is close enough to the melt curve, the release isentrope intersects it. At this intersection, the tin initially becomes a mixed phase of solid and liquid at the melting temperature for that pressure. While the pressure and temperature continue to drop, the release isentrope follows a segment of the melt boundary to low pressures as the liquid fraction of the phase mixture increases. With our geometry, the release rate is low enough (about 75 GPa/μs) that it is time resolved by our instruments. Table I gives the shock parameters for four radiance (R) and four emissivity (E) experiments. Shock pressures are calculated from the velocity measurements using the stress vs particle velocity relationship for LiF,[24] and we have assumed that the material strength is negligible in our experiments so that the longitudinal stress and the pressure are equal for both the tin sample and the LiF window. The interface pressure values listed in Table I occur immediately prior to the arrival of the release wave. The pressure and temperature values for the first melt are determined from the change in slope of the P-T release curves (see Sec. III).

III. RESULTS AND DISCUSSION

Shown in Fig. 3 are the measured radiance and velocimetry data from experiment 2R and reflectance and velocimetry from experiment 2E, both for an initial pressure of ~26.3 GPa at the interface. When the shock reaches the tin-window interface, the tin at the surface transforms almost immediately to the γ phase, and with this phase change, the tin's reflectance increases from 5% to 15%.[25] About 600 ns later, there is a subsequent drop in reflectance when the shock release reaches the tin melting point. These sudden emissivity changes indicate that, at least for tin, the reflectance alone marks the onset of the phase change during shock release. We suggest that other metals, too, often have reflectance values that differ for different phase states.

The ambient spectral reflectance R_0 of the tin-LiF interface is measured before every experiment on a commercial IS instrument by comparing the reflectance to a calibrated standard. During analysis of the experiment, the measured detector voltage is normalized to the signal just before shock breakout. The normalized signal, V/V_0, is equal to the relative reflectance change, R/R_0. Multiplying the normalized signal by R_0 gives the dynamic reflectance, which is converted to dynamic emissivity through the relation $\varepsilon = 1 - R$. Combining the dynamic emissivity and radiance data into Planck's law, we determine the temperature vs time for each of the two wavelengths, verify that they agree, and combine the two curves statistically using the methods described in La Lone.[20] Uncertainties in the measured interface temperatures for each experiment are estimated to be ±4% or less.

The temperature determined from the radiance and reflectance measurements is plotted vs the shock pressure as derived from the velocimetry. Figure 4 shows the measured temperature-pressure data along the release isentropes for all of our experiments. The temperature curves as shown release from right to left.

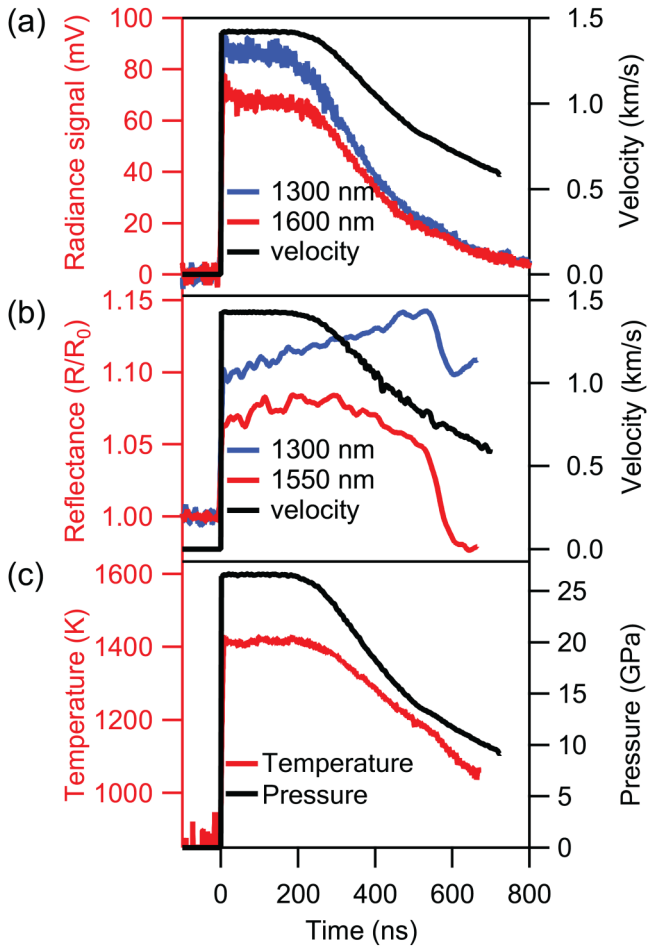

FIG. 3. (a) Velocity and radiance signals for experiment 2R, and (b) velocity and the ratio of dynamic to static reflectance for experiment 2E. The shock arrives at the interface at time 0, and the experiment ends when the shock reaches the back of the window, around 700 ns. The onset of melt occurs at 580 ns in the reflectance data and less obviously in the radiance. (c) The radiance and reflectance measurements are combined to generate a temperature vs time trace.

Experiment 1R began at pressure and temperature values too low to intersect the melt curve during the release, so the tin remained in the solid phase. For experiments 2R and 3R, the release isentropes do intersect the melt boundary. There the slope changes, becoming sharply steeper, as the release isentrope becomes confined to the melt boundary. The measured release isentropes for the different experiments, starting from different temperature and pressure conditions, overlap each other in this steeper section. The overlap of two different constant entropy paths in temperature-pressure space is only possible at a phase boundary because the difference in phase fractions can account for the entropy differences. Therefore, the observed overlap is further evidence of the melt boundary location. Experiment 4R begins very near to, or perhaps on, the melt boundary and stays on it for the majority of the

release. Below about 16 GPa, the release isentrope for experiment 4R decreases in slope again and maintains slightly higher temperatures than the other curves at the same pressures. We interpret this segment as having reached complete melting so that the release departs from the melt boundary and enters the liquid phase region.

We fit a Simon-Glatzel melt function to the portions of our release paths believed to be on the melt curve. The function has the form

$$T_{melt} = T_{triple}\left(\frac{P_{melt} - P_{triple}}{A} + 1\right)^{\frac{1}{C}}, \quad (1)$$

where we used the triple-point[8] values $T_{triple} = 562$ K and $P_{triple} = 3.02$ GPa; we found best-fit values of $A = 3.244 \pm 0.013$ GPa and $C = 1.885 \pm 0.003$. This curve defines the boundary between the color-coded solid and liquid phase fields in Fig. 4. As seen in Fig. 1, our melt curve data for tin are in agreement with the Mabire and Héreil,[10] Xu *et al.*,[8] and Bernard and Maillet[15] calculations, but they are above the Mukherjee *et al.*[16] calculations and disagree slightly with the new SESAME EOS calculations. These data show that with this technique, we can determine a large, continuous section of a melt curve with a single measurement of reflectance and radiance (or a pair of separate measurements). A further advantage of our method, compared to other shock wave techniques, is that we measure the melting temperature accurately, not just the pressure at which melting occurs. Two limitations of our technique are that the initial shock pressure must be on or below melt on the Hugoniot (about 45 GPa for tin) and that we must know approximately where in phase space to look for the phase boundary; therefore, the experiments must be guided by prior modeling and experimental efforts. In principle, methods are available and could be used to expand the accessible P-T range along the melting curve by altering the initial conditions (temperature or pressure) or the loading path (ramp compression, multiple shocks, etc.).

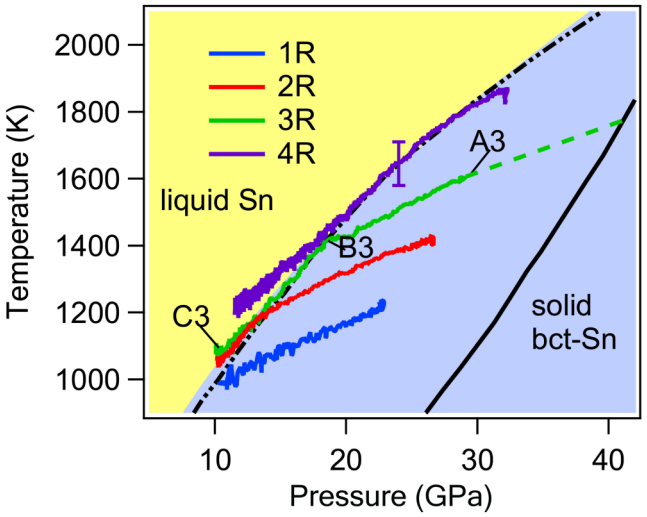

FIG. 4. Measured temperature vs pressure release isentropes (solid colored lines). The experiment begins when the shock reaches the tin-LiF interface (point A3 for measurement 3R). After a dwell time of about 300 ns at the shock state, the rarefaction wave arrives and the tin-LiF interface releases isentropically (right to left). At point B3, the 3R release isentrope intersects the melt curve, changing the slope of the release path. Subsequent release is along the melt curve until the initial shock reaches the back of the LiF window, ending the useful data at point C3. The error bar on the 4R curve and the width of the pink curve in Fig. 1 show a representative absolute temperature uncertainty of about 4%, which is typical for all measurements. (The point-to-point noise within an experiment and the error on relative temperature differences between experiments are much less than 4%). The boundary between the liquid region (yellow shading, left) and the solid region (blue shading, right) is determined by a Simon-Glatzel fit to the segments of the experimental release paths believed to be on the melt curve. The black dotted-dashed curve is a model calculation from Mabire and Héreil,[10] which is also shown in Fig. 1 and is in general agreement with our results, although at the lowest pressures it is at the low limit of our uncertainty band. The solid black line is the shock Hugoniot calculation from Mabire and Héreil.[10] The shocked tin initially compresses onto the Hugoniot but releases abruptly (see the dashed green curve for 3R) at the tin-LiF interface due to the impedance mismatch between tin and the LiF window; therefore, the measured paths begin at a lower stress than the Hugoniot.

Temperatures we measure are not necessarily in thermal equilibrium with the bulk, or sample interior, and are not perfectly on the isentrope starting at the shock Hugoniot point because of the potentially nonisentropic wave reverberations in the glue layer and because of heat conduction between the interface and the bulk tin and/or the glue.[20,26] We estimate that the measured interface temperatures differ by up to 50 K from the interior release isentrope temperatures due to these interface effects.[20] Note that the <50 K difference is only important for the release isentrope in the solid phase and not important for the melt measurement. The interface itself, where we observe the temperature and pressure, is partially melted and, therefore, on the melt curve.

IV. SUMMARY

We have developed a method to measure the high-pressure melt curve of a metal by combining reflectance, pyrometry, and velocimetry measurements to determine temperatures and pressures during dynamic shock compression and release experiments. In principle, such a measurement can be made with two experiments, a measurement of the reflectance at two or more wavelengths using an integrating sphere and a pyrometric measurement of the shock radiance with the same or a similar set of detectors. We executed several experiments at different shock conditions to help understand the reproducibility of the measurements.

By measuring the temperature vs pressure as the metal releases isentropically from the shocked state, we have directly observed a large segment of the tin melt boundary as indicated by a change in slope of the release $T(P)$. For tin, we have also found that the reflectivity alone is an indicator of the onset of melt because the reflectance changes abruptly at the point where the shock release isentrope and melt curves intersect. We have obtained accurate temperature data for tin across a significant region of the phase diagram, from 1000 to 1800 K from about 10 to 30 GPa, and we compared our result to previous determinations of the melt curve and the predictions of standard EOS models from the literature. These techniques will enable similar temperature measurements in the phase change regime for other metals. The glue layer limits the peak stresses and, therefore, the present technique is only

applicable to somewhat low melting point metals that melt when shocked to below approximately 70 GPa (depending on shock impedance) and released. We are exploring methods that omit the glue layer such as mechanically pressing the window and sample together or vapor depositing the sample onto the window. Omitting the glue will enable melt boundary measurements with our technique on high temperature and pressure melting metals.

In future experiments at higher stresses, we will explore more of the melt curve of tin. Starting from higher shock stresses and temperatures, we expect the release isentrope to eventually depart from the melt curve and continue to unload into the liquid phase region. These techniques will enable similar temperature measurements in the phase change regime for other metals, and we anticipate measuring the iron melt curve, where previous dynamic pyrometric measurements have uncertainties of ±500 K[27] and ±900 K.[28]

ACKNOWLEDGMENTS

We are grateful for the help of Michael Burns, Russel Oliver, Ben Valencia, Mike Grover, Roy Abbott, Rick Allison, and Matthew Staska in performing the experiments.

This manuscript has been authored by Mission Support and Test Services, LLC, under Contract No. DE-NA0003624 with the U.S. Department of Energy and supported by the Site-Directed Research and Development Program, National Nuclear Security Administration, NA-10 USDOE NA Office of Defense Programs (NA-10). The United States Government retains and the publisher, by accepting the article for publication, acknowledges that the United States Government retains a non-exclusive, paid-up, irrevocable, worldwide license to publish or reproduce the published form of this manuscript, or allow others to do so, for United States Government purposes. The U.S. Department of Energy will provide public access to these results of federally sponsored research in accordance with the DOE Public Access Plan (http://energy.gov/downloads/doe-public-access-plan). The views expressed in the article do not necessarily represent the views of the U.S. Department of Energy or the United States Government. DOE/NV/03624–0470.

REFERENCES

[1]As an example for the melt data for tantalum, see C. Dai, J. Hu, and H. Tan, J. Appl. Phys. **106**, 043519 (2009).
[2]J. D. Dudley and H. T. Hall, Phys. Rev. **118**, 1211 (1960).
[3]G. C. Kennedy and R. C. Newton, in *Solids Under Pressure*, edited by W. Paul and D. M. Warschauer (McGraw-Hill, New York, 1963), Chap. 7.
[4]R. A. Stager, A. S. Balchan, and H. G. Drickamer, J. Chem. Phys. **37**, 1154 (1962).
[5]J. D. Barnett, V. E. Bean, and H. T. Hall, J. Appl. Phys. **37**, 875 (1966).
[6]B. Schwager, M. Ross, S. Japel, and R. Boehler, J. Chem. Phys. **133**, 084501 (2010).
[7]S. T. Weir, M. J. Lipp, S. Falabella, G. Samudrala, and Y. K. Vohra, J. Appl. Phys. **111**, 123529 (2012).
[8]L. Xu, Y. Bi, X. Li, Y. Wang, X. Cao, L. Cai, Z. Wang, and C. Meng, J. Appl. Phys. **115**, 164903 (2014).
[9]R. Briggs, D. Daisenberger, O. T. Lord, A. Salamat, E. Bailey, M. J. Walter, and P. F. McMillan, Phys. Rev. B **95**, 054102 (2017).
[10]C. Mabire and P. L. Héreil, AIP Conf. Proc. **505**, 93 (2000).
[11]P.-L. Héreil and C. Mabire, J. Phys. IV France **10**, 799 (2000).
[12]W. W. Anderson, F. Cverna, R. S. Hixson, J. Vorthman, M. D. Wilke, G. T. Gray, and K. L. Brown, AIP Conf. Proc. **505**, 443 (2000).
[13]D. B. Hayes, J. Appl. Phys. **46**, 3438 (1975).
[14]C. Chauvin, Z. Bouchkour, F. Sinatti, and J. Petit, AIP Conf. Proc. **1793**, 060013 (2017).
[15]S. Bernard and J. B. Maillet, Phys. Rev. B **66**, 012103 (2002).
[16]D. Mukherjee, K. D. Joshi, and S. C. Gupta, AIP Conf. Proc. **1349**, 821 (2011).
[17]C. Greeff, E. Chisolm, and D George, Los Alamos National Laboratory Report No. LA-UR-05-9414, 2005.
[18]B. M. La Lone, G. Capelle, G. D. Stevens, W. D. Turley, and L. R. Veeser, Rev. Sci. Instrum. **85**, 073903 (2014).
[19]A. Seifter, M. Grover, D. B. Holtkamp, A. J. Iverson, G. D. Stevens, W. D. Turley, L. R. Veeser, M. D. Wilke, and J. A. Young, J. Appl. Phys. **110**, 093508 (2011).
[20]B. M. La Lone, G. D. Stevens, W. D. Turley, D. B. Holtkamp, A. J. Iverson, R. S. Hixson, and L. R. Veeser, J. Appl. Phys. **114**, 063506 (2013).
[21]Vulcan Resources, Inc., Phoenix Arizona, 99.9% purity tin with 100 μm average grain size.
[22]M. C. Akin and R. Chau, J. Dyn. Behav. Mater. **2**, 421 (2016).
[23]O. T. Strand, D. R. Goosman, C. Martinez, and T. L. Whitworth, Rev. Sci. Instrum. **77**, 083108 (2006).
[24]S. P. Marsh, *LASL Shock Hugoniot Data* (University of California Press, Berkeley, CA, 1980).
[25]W. D. Turley, D. B. Holtkamp, L. R. Veeser, G. D. Stevens, B. R. Marshall, A. Seifter, R. B. Corrow, J. B. Stone, J. A. Young, and M. Grover, J. Appl. Phys. **110**, 103510 (2011).
[26]R. Grover and P. A. Urtiew, J. Appl. Phys. **45**, 146 (1974).
[27]C. S. Yoo, N. C. Holmes, M. Ross, D. J. Webb, and C. Pike, Phys. Rev. Lett. **70**, 3931 (1993).
[28]G. Huser, M. Koenig, A. Benuzzi-Mounaix, E. Henry, T. Vinci, B. Faral, M. Tomasini, B. Telaro, and D. Batani, Phys. Plasmas **12**, 060701 (2005).